Virtual Magnetic Resonance Imaging – Parallel Implementation in a Cluster Computing Environment

KRZYSZTOF JURCZUK*, MAREK KRĘTOWSKI

Faculty of Computer Science, Białystok Technical University, Białystok, Poland

In this paper, we present a virtual scanner of magnetic resonance imaging that aims at simplifying and accelerating methods of generating images. After an introduction to the subject of nuclear magnetic resonance and various approaches to the simulation of magnetic resonance imaging, details of the simulator are described. The proposed simulator consists of magnetization kernel (based on a solution of the Bloch equation), graphical user interface and module that performs calculation in a parallel environment. The package which parallelizes the magnetic resonance simulation is implemented on a computing cluster with the use of the Message Passing Interface standard. The parallel module can divide calculations related to different slices or different phase encoding steps between processors. The experimental results in the parallel environment show that it is possible to gain a significant speedup thus making it possible to acquire more exact images in a reasonable period of time.

K e y w o r d s: medical imaging, simulation of magnetic resonance imaging, cluster computing

1. Introduction

Magnetic resonance imaging (MRI) is one of the most popular tomography method which has revolutionized diagnostic imaging in medical science [1]. It is based on the principles of nuclear magnetic resonance (NMR), a spectroscopic technique used by scientists to obtain microscopic chemical and physical information about molecules. The NMR phenomenon was independently discovered by Bloch [2] and Purcell [3]. One of MRI advantages is the possibility to produce images characterized by high spatial resolution. Moreover, it provides unique contrast between soft tissues, which is generally superior to that of computed tomography (CT). So far, it seems to be a non-invasive method, especially in comparison to CT or positron emission tomography (PET).

However, MRI scanners, despite of a considerable number of advantages, are still inaccessible for research to many scientists and physicians. This is partly due to high cost of the equipment and also necessity to employ skilled personnel to operate and maintain MRI machines. Therefore, it appears natural to attempt to build simulators of magnetic resonance imaging as they can effectively eliminate high cost connected with specialist, physical devices. Moreover, the simulators allow us to perform simulations with no need for patients to participate and thus as long as we wish. They not only enable testing, development and optimization of the parameters of actual equipment but also facilitate research on new image acquisition techniques. As the simulation is one of the easier ways to comprehend the complex principles of NMR, virtual scanners can be used as an education tools both in medical and technical environments.

So far, there have been a few MRI virtual scanners proposed. One of the first MRI simulators solving the Bloch equation at each point of an object was the one proposed by Bittoun [4]. Later, it was improved by Summers [5] and Olsson [6]. Unfortunately, this approach quickly became computationally inefficient, even in the parallel environment [7], because of increasing necessity to simulate high resolution images. Consecutive simulators used image intensities for different pulse sequences [8] and [9]. However, this approach makes it impossible to simulate most of artifacts encountered in magnetic resonance images, e.g. chemical shift and magnetic field inhomogeneity. Another type of virtual scanners used k-space formalism [10]. Such a simulator transformed a spin density image to the k-space amplitudes which, after some corrections, can be used to simulate the selected pulse sequence, relaxation and motion. The use of this transformation implies the close relationship between the sampling frequency and the field of view. Moreover, in this approach there were problems with non-uniform tissue characteristics, because it treats each tissue separately. The latest and the most modern type of simulators is based on discrete solutions of the Bloch equation as [11] and [12]. This approach is the closest to reality and allows simulating most of the MRI artifacts (e.g. chemical shift, static field inhomogeneity, etc.).

In our previous studies [13] and [14] concerned with the search for pathology markers and improving the interpretation of dynamic medical images, a CT simulator was used. At present, with the increasing demands on MRI investigation due to its many advantages, we have decided to continue research with magnetic resonance images. According to the acquired knowledge and conducted trials, most of the recently proposed MRI simulators are capable of simulating high-quality images that take into account many NMR principles. However, very often they are cumbersome or inefficient in research because of high complexity or small flexibility. Moreover, many people from outside the computer science environment encounter problems with using them, especially when choosing MRI parameters or storing results. On the other hand, other simulators which are computationally faster do not take into consideration enough details and consequently they are not realistic enough. As a result,

in this paper, an MRI simulator that would both simplify and accelerate methods of generating images in proposed. Special attention is paid to the most important NMR principles which are essential for tissue contrasting, whereas the remaining ones of lesser significance were disregarded (e.g. direct impact of oscillating radio frequency pulse on the received signal). Furthermore, both a user-friendly graphical interface and a module to parallelize the most complex computations in the magnetization kernel were created. At the same time attempts to build a simulator that would enable us to obtain images as close to real images as possible were made.

The remaining part of the paper is organized as follows. In the next section the NMR phenomenon is discussed. In section 3 a mathematical model of the simulator is presented, whereas section 4 describes the environment of virtual scanner, including parallel implementation and graphical user interface. An experimental validation of the presented approaches is performed in section 5. The conclusion and some plans for future research are sketched in the last section.

2. NMR Fundamentals

The NMR phenomenon can be observed when particles with nonzero magnetic moments are placed in static magnetic field B_0 and are irradiated by an oscillating magnetic pulse B_1 [15]. In the presence of static magnetic field their nuclear moments align with the lines of magnetic field in two ways: either parallel or anti-parallel. Additionally, they start to precess in the plane perpendicular to B_0 [T] (see Fig. 1a) at an angular frequency ω_0 [Hz] described by the Larmor equation:

$$\omega_0 = \gamma B_0, \tag{1}$$

where γ [Hz $\cdot$ T^{-1}] is the gyromagnetic ratio. The distribution of the particles for both states is not the same. There are more nuclei aligned parallel (low energy level) than
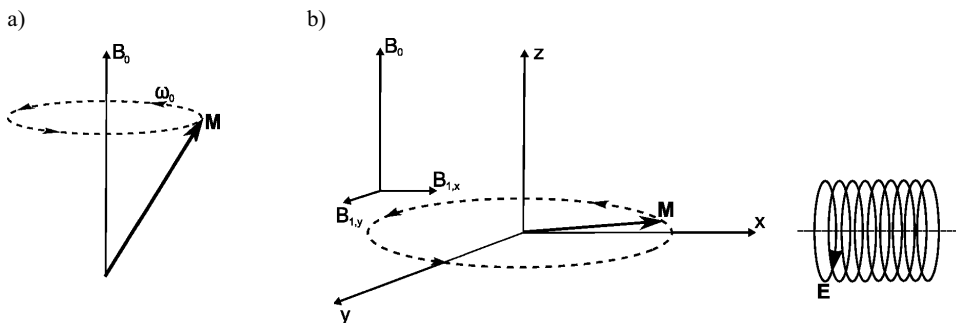

Fig. 1. Behavior of the resultant magnetization vector M in the presence of: a) main magnetic field B_0, b) main magnetic field B_0 and oscillating radio frequency pulse B_1 (induction of voltage E in a coil of wire and ω_0 frequency of precession)

anti-parallel (high energy level). However, the difference is very small (e.g. 3 per million with 0.5 Tesla field [15]). Additionally, after a perturbation by an oscillating magnetic field, whose frequency must be equal or very close to the frequency of precession ω_0, particles in a low energy state can absorb energy and pass to a higher energy state. This process is known as excitation and this can be the reason why resultant magnetization appears in the plane perpendicular to the B_0 plane, due to equal number of particles in both low and high states and the same phase shift in their precession around B_0.

After the pulse is turned off, the transverse magnetization decays because of nuclear interactions and B_0 nonuniformity. This process is called a transverse or T2 relaxation. At the same time particles start to release the absorbed energy and a recovery of longitudinal magnetization, called a longitudinal or T1 relaxation is observed. The time-varying magnetization induces voltage in the coil (see Fig. 1b). The received signal is known as Free Induction Decay (FID). The behavior of the transverse and longitudinal magnetization is specific for each tissue and it depends on $T1$ and $T2$ constants as follows:

$$M_z(t) = M_0(1 - e^{-t/T1}), \tag{2}$$

where M_z [A·m^{-1}] is the longitudinal magnetization and M_0 [A·m^{-1}] is the equilibrium magnetization, and:

$$M_{xy}(t) = M_0 e^{-t/T2}, \tag{3}$$

where M_{xy} [A·m^{-1}] is the transverse magnetization. These differences in the speed of the longitudinal and transverse relaxations allow contrasting various tissues and tumors in images created from FID signals.

It should be noted that for most typical magnetic field strengths used in MRI and spectroscopy (from about 0.5 to 3 Teslas), the resonance frequencies belong to the radio frequencies of the electromagnetic spectrum. Therefore, we often call additional pulse B_1 as a radio frequency pulse. This is one of the main reasons why the MRI technique is non-invasive, especially in comparison to CT or PET.

3. Modeling of Magnetic Resonance Imaging

Generally, to model the process of imaging two elements are necessary: a virtual organ and a simulator [16]. The modeling quality of these two elements has a crucial influence on simulated images. Hence, it seems to be important to take into account as many details as possible. On the other hand, too elaborate models can be ineffective in practical cases as the computations cannot be carried out in a reasonable time. As a result, we decided to concentrate on the most important MRI factors which

have the most significant influence on the tissue contrasting and tumor recognition (e.g. relaxations, different sequences) and disregard others (e.g. radio frequency inhomogeneity, non-linearity of coding gradients) [17].

Figure 2 presents an overview of the proposed solution. The virtual organ is placed in the main magnetic field of the simulator and submitted to the radio frequency pulse. If the conditions of the nuclear magnetic resonance are fulfilled, a series of matrixes containing signals in the form of induced voltage in the receiver coils are collected. At the end, the image reconstruction is performed.
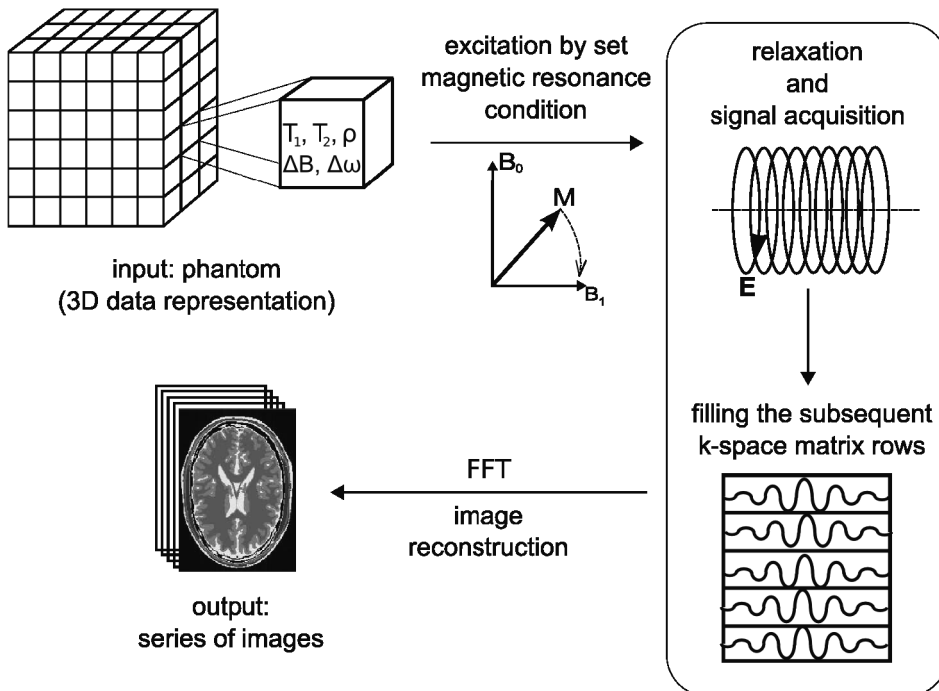

Fig. 2. Overview of the proposed solution of MRI modeling. Virtual object (phantom) represented by fixed-size voxels is placed in B_0 and B_1 magnetic field. If magnetic resonance conditions are fulfilled, the MRI simulation is performed (relaxation and signal acquisition). In order to obtain an image the fast Fourier transform is carried out

The next part of section 3 describes the model of magnetic resonance imaging simulation followed by the presentation of virtual organ description.

3.1. MRI Simulator

The mathematical model of the proposed virtual scanner consists of three components. The first is used to simulate the excitation and relaxation processes. The second is responsible for the signal acquisition and the last reconstructs images.

The model allows us to change the thickness of slices, repetition time (TR), echo time (TE), inversion time (TI), sampling interval (ΔTs), sampling time (Ts), frequency encoding range, number of frequency encoding steps, phase encoding range, number of phase encoding steps, flip angle (FA), etc. Moreover, there is a possibility to choose one of the three following sequences: spin echo (SE), gradient echo (GE) or inversion recovery (IR).

3.1.1 Magnetization Kernel

Modeling of the excitation and relaxation processes, during a magnetic resonance experiment, is based on the discrete time solutions of the Bloch equation [18]. It describes the evolution of the spin magnetization vector $\mathbf{M} = (M_x,\ M_y,\ M_z)^T$ in time t:

$$\frac{d\mathbf{M}(t)}{dt} = \gamma(\mathbf{M}(t) \times \mathbf{B}) - i\frac{M_x(t)}{T_2} - j\frac{M_y(t)}{T_2} - k\frac{M_z(t) - M_0}{T_1}, \tag{4}$$

where $\mathbf{M}(t)$ is the magnetization vector at time t, $\mathbf{B}(t)$ [T] is the magnetic field at time t, $T1$ and $T2$ are the relaxation times and i, j, k are the versors of perpendicular axes x, y, z. The induction of the whole magnetic field that has an influence on the imaged object is decomposed as follows:

$$\mathbf{B}(\mathbf{r}, t) = B_0 k + \Delta B(\mathbf{r})k + \mathbf{G}(\mathbf{r}, t) + \mathbf{B_1}(t), \tag{5}$$

where $\Delta B(\mathbf{r})$ [T] is the magnetic field inhomogeneity, $\mathbf{G}(\mathbf{r}, t)$ [T] are the magnetic gradients, $\mathbf{B_1}(t)$ [T] is the magnetic induction of radio frequency field and $\mathbf{r} = (x, y, z)^T$ is the position in space. In further parts of the proposed model the component connected with the magnetic field B_1 is disregarded (complexity reduction), due to its short duration in comparison with relaxation times and a small value of its magnetic induction with respect to main magnetic field B_0 value.

The chemical shift is defined by using the dimensionless unit of parts per million (ppm) [15]:

$$\delta = \frac{\omega_i - \omega_w}{\omega_w}10^6, \tag{6}$$

where ω_i [Hz] is the resonance frequency of given nuclei and ω_w [Hz] is the arbitrary chosen reference frequency.

The received signal, as a result of the relaxation processes, comes from the entire volume which has been excited. In order to code the spatial position which enables us to identify the exact source of signal two magnetic gradients are used: phase encoding and frequency encoding.

The signal received in the MRI experiment is a voltage induced in a coil of wire. It results from changes in the magnetic field flux created by displacements of magnetic vectors of the excited particles. This relation was described by the Faraday's law of an electromagnetic induction [17]. Basing on the law, the equation to simulate the voltage $E(t,t_1)$ [V] from the whole excited volume V is modeled as follows:

$$E(t,t_1) = -\int \mu_0 \frac{N}{L} \frac{\sigma \mathbf{M}(\mathbf{r},t,t_1)}{\sigma t} dV, \qquad (7)$$

where μ_0 [H · m^{-1}] is vacuum permeability and t_1 is the time connected with a phase encoding gradient. For simplicity's sake we assume the receiver to be a long cylindrical coil of length L with N turns encompassing a sample of volume. It lies in a plane perpendicular to the magnetic field B_0, that makes it possible to neglect the direct influence of this field on the received signal which leads to the reduction of complexity (changes of longitudinal magnetization are only necessary during the calculations of the initial values of magnetization and the model simulates them by signal intensities).

The simulated voltage, after an analog-digital conversion, becomes a one-dimensional discrete and complex signal that fills one k-space matrix row (k-space matrix is a spatial frequency representation of information about scanned objects, in which each position is directly related to the applied gradient [19]). Each subsequent excitation is performed with a different phase encoding step and the received signal fills the next matrix row. The middle row contains the signal with maximum amplitude (maximum information) because it is filled without additional dephasing due to the phase encoding gradient. Consecutive rows are obtained with progressively larger gradients, therefore they possess signals with weaker amplitudes.

3.1.3. Image Reconstruction

The MRI experiment ends when the required number of excitations has been performed. The k-space matrix contains all information needed to create image, however, it is spatially encoded. Therefore, to obtain an image the Fourier transform algorithm is performed. Because of lower computation complexity, a modified version of the algorithm is applied, called the fast Fourier transform [20].

3.2. Virtual Object Description

The virtual object consists of fixed-size voxels. Each voxel contains information necessary to compute a local spin magnetization. These values are: proton density, spin-lattice relaxation time (T1), spin-spin relaxation time (T2), optionally magnetic

field inhomogeneity, and difference in resonance frequency connected with a chemical shift effect. When one voxel is composed of more than one tissue, we have to define a proportion for each tissue and give discrete values of the above-mentioned parameters.

4. Environment for MRI Simulations

The MRI virtual scanner is implemented in the C++ programming language. The simulator consists of a library based on the mathematical model and responsible for imaging, the graphical user interface (GUI) developed in MFC .NET 2005, and a module for the calculations in a parallel environment implemented on a computing cluster with the use of the MPI standard [21] (see Fig. 3).
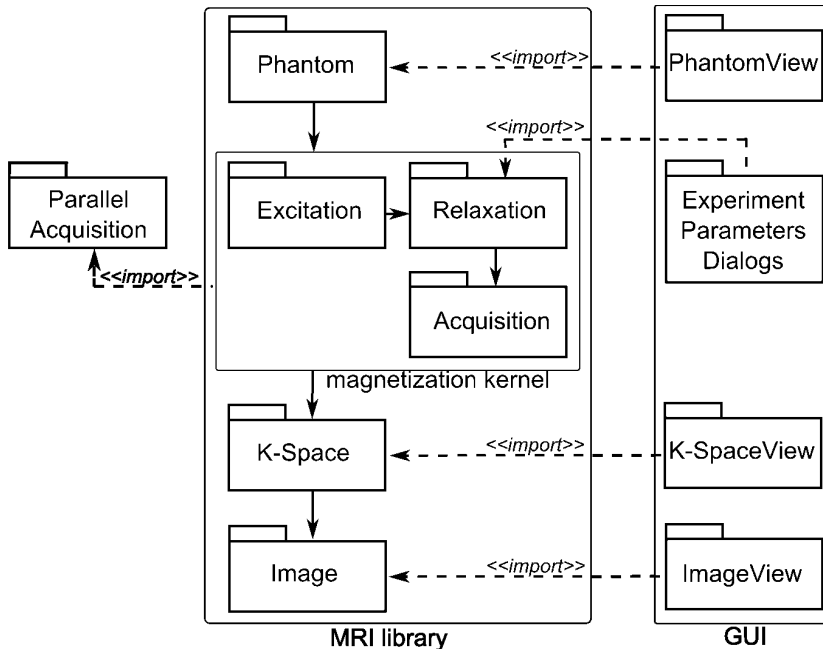

Fig. 3. Package diagram for simulator module arrangement (solid lines with arrows determines a package usage order during the standard MRI simulation)

The MRI simulation starts with defining a virtual object (Phantom package) and next the MRI experiment is performed in the following order: an excitation process (Excitation package), relaxation process (Relaxation package) and acquisition process (Acquisition package). As a result, a k-space matrix with signals is produced

(K-Space package). Finally, an image reconstruction is performed (Image package). If we want to execute the computations in a parallel environment, the ParalellAcquisition package is used. The package GUI allows viewing in dialog windows: virtual objects (PhantomView package), k-space matrixes (K-SpaceView package) and images (ImageView package). Moreover, the package ExperimentParametersDialogs enables users to choose an MRI simulation method and its parameters in the dialog windows.

4.1. Parallel Implementation

The MRI simulation is a process which is characterized by high complexity. In order to find the most time consuming operations we used a profiling software which allows developers to gain valuable metrics (e.g. memory usage and execution times of specific methods) and provides a detailed insight into the performance of the application. In our case, the profiling of the execution of the proposed virtual scanner showed that the computations in the magnetization kernel takes on average 90% of the whole time needed to create an image. Moreover, we noted that the most time consuming operation is the signal acquisition process. Therefore, it appears natural to attempt to use parallel computing.

In the proposed simulator each subsequent signal acquisition process connected with different phase encoding steps is independent. Furthermore, during a multislice imaging each slice is independent. Therefore, a decision was made to focus the attention on two issues. Firstly, to accelerate the process of the calculations in a single slice and secondly, to speedup the computations during a multislice simulation.
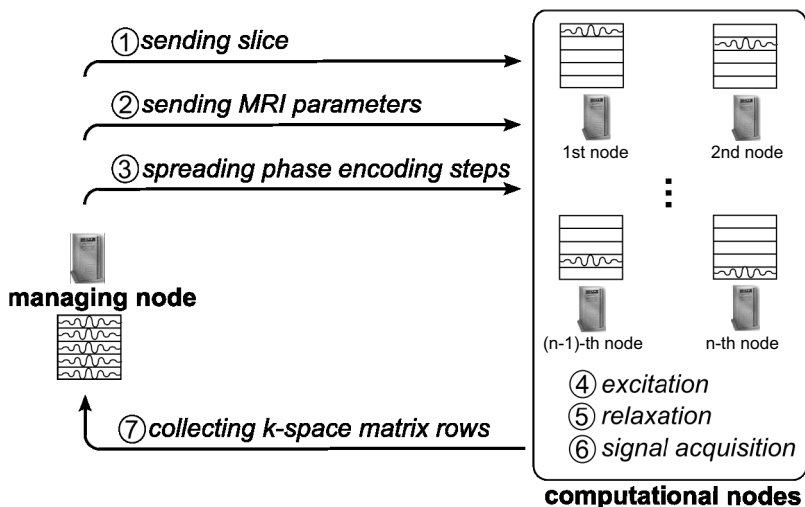

Fig. 4. Schematic diagram of the parallel algorithm for a single slice simulation

In the first approach (during a single slice simulation, see Fig. 4), each calculation node must possess a selected part of the virtual organ. Therefore, at the beginning the managing node broadcasts the same slice over calculation nodes. The process of voxel migration (transverse relaxation time, longitudinal relaxation time, proton density, etc.) with the framework of the message passing interface is composed of three steps: packing the characteristics into a flat message, transferring the message between processors and unpacking the corresponding values of the slice. Additionally, all computation nodes receive the MRI experiment parameters (TR, TE, FA, etc.). Next, the managing node spreads phase encoding steps between all nodes which, in turn, simulate signals that fill different k-space rows. In the end, calculation nodes send the obtained information to the managing node which puts signals in an appropriate order in the receiving matrix and performs the image reconstruction process.

In the second approach (during a multislice simulation, see Fig. 5), each calculation node is responsible for different slices. At the beginning, the managing node spreads different parts of the virtual organ and broadcasts the same MRI sequence parameters over calculation nodes. Next, each calculation node performs all tasks needed to collect the MRI signals from the received slices, which means all the calculations connected with the whole phase encoding range. In the end, the managing node gathers the k-space matrixes and applies the image reconstruction algorithm.

In the proposed solution it is possible to combine two presented approaches. The calculation node from the second approach can become the managing node from the first approach. Moreover, it is worth noting that the managing node performs the same calculations as the other nodes, instead of waiting for results.
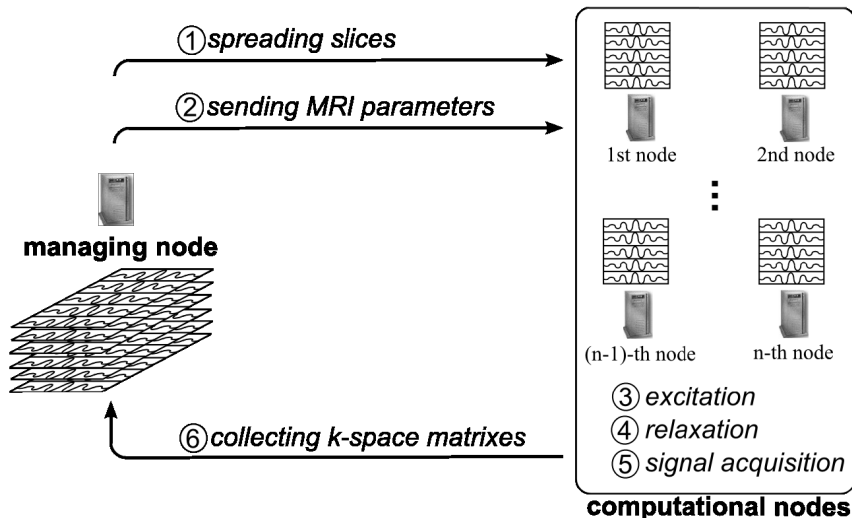

Fig. 5. Schematic diagram of the parallel algorithm for a multislice simulation

4.2. User-friendly Graphical Interface

We created the graphical user interface to our scanner in order to simplify and accelerate the procedure of virtual imaging. Part of the GUI is showed in Fig. 6. It allows users to load and display the imaged 3D phantoms, perform the simulation of the imaging and, finally, to visualize and compare the simulation results. Moreover, one can choose the MRI sequence and its parameters in dialog windows. The implemented module proposes appropriate values for certain parameters (e.g. phase encoding range and step, frequency encoding range and step) to avoid artifacts related to the spatial encoding or analog-digital conversion. Additionally, there is a possibility to create difference images using the results from other simulators. Furthermore, the proposed simulator makes it possible to choose the region of interest to be scanned. This can be very useful when we need to find appropriate parameters of the selected MRI sequence as it allows performing a quick prescan on a small, fixed part of the phantom.
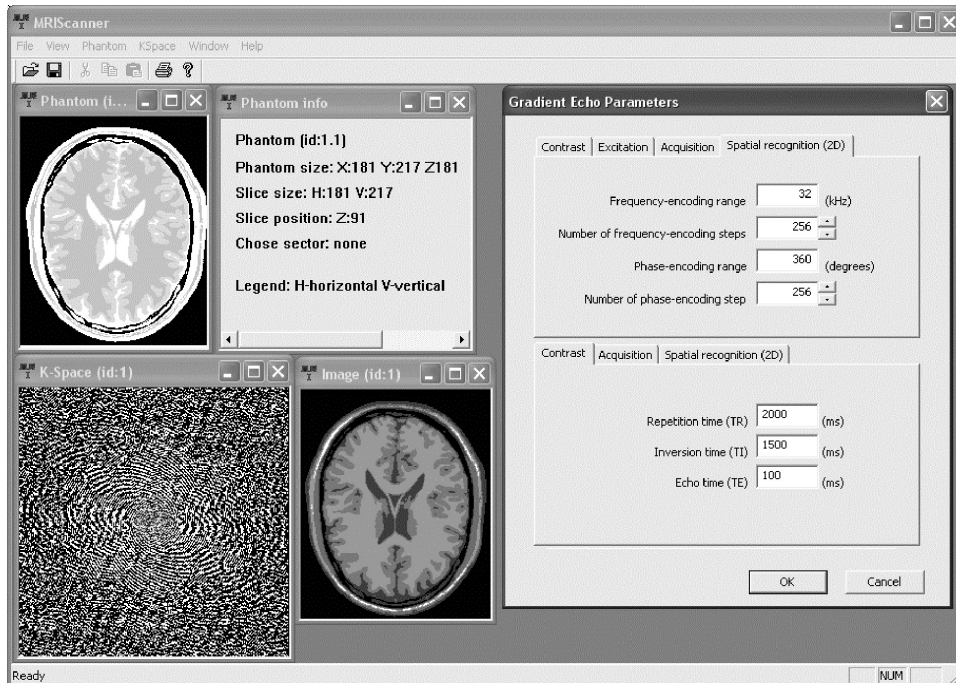

Fig. 6. Overview of the main window of the MRI simulator with some results of the brain phantom

5. Experimental Results

In this section the proposed virtual scanner is experimentally verified. At the beginning, we describe the validation of the simulator and then we investigate the efficiency of a parallel implementation.

5.1. Validation of the Simulator

One of the most objective methods to validate imaging simulators is to compare images of real phantoms with simulated images of their equivalents (virtual phantoms). However, due to difficulties in obtaining and building real phantoms and a limited access to the MRI scanners, we decided to validate the proposed simulator by comparing the created images with the results from two other virtual scanners. To make the comparison easier difference images (absolute value from difference between images) were formed.

As the first scanner, we used SIMRI [12], a versatile and interactive MRI simulator. Figure 7 presents one of the representative results. The difference image shows that there are some deviations, especially in a neighborhood of a tissue borders (mean difference equals 15.1 and median difference equals 7 in 256 gray shades). We suppose that these differences can be caused by an additional noise which the SIMRI adds to a k-space matrix and then tries to filter it out.
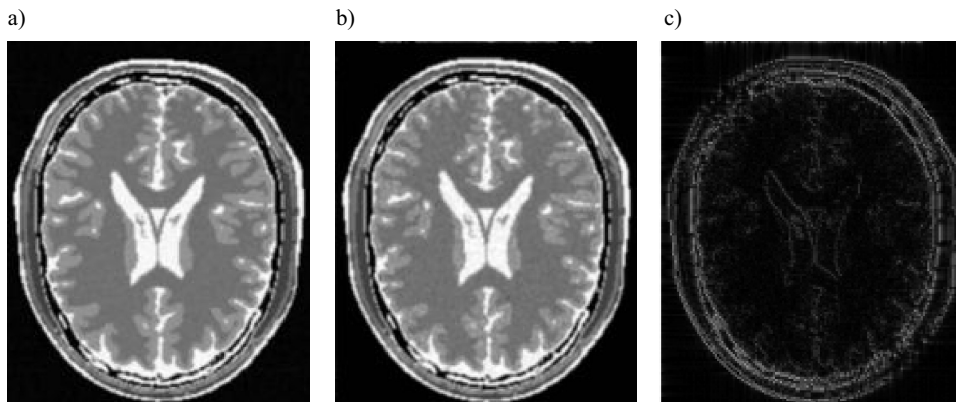
a)   b)   c)

Fig. 7. Validation of the simulator, images generated in a spin echo experiment (TR = 2000ms, TE = 100ms): a) from the presented simulator, b) from SIMRI and c) difference image (absolute value from difference between image a) and b))

The second simulator is a solution proposed by "McConnell Brain Imaging Center" at Montreal University [11]. The difference image also shows insignificant variations situated close to tissue borders (mean difference equals 12.6 and median difference equals 8.36 in 256 gray shades, see Fig. 8), similarly to the case of the SIMRI. The source code of the simulator from Montreal University is unavailable (we can use this scanner via web page interface), therefore the differences cannot be precisely analyzed. We can only guess that these deviations come from a different approach in the magnetization kernel, noise or partial volume effects.

Moreover, our simulator has been used in research connected with the process of detection of pathological anomalies (especially hepatocellular carcinoma, the

most common malignant tumor of the liver [22] and [23]). We tried to analyze the contrast product propagation and find markers of the pathologies. The generated images, both with and without a contrast product administration, were convergent to the real images.
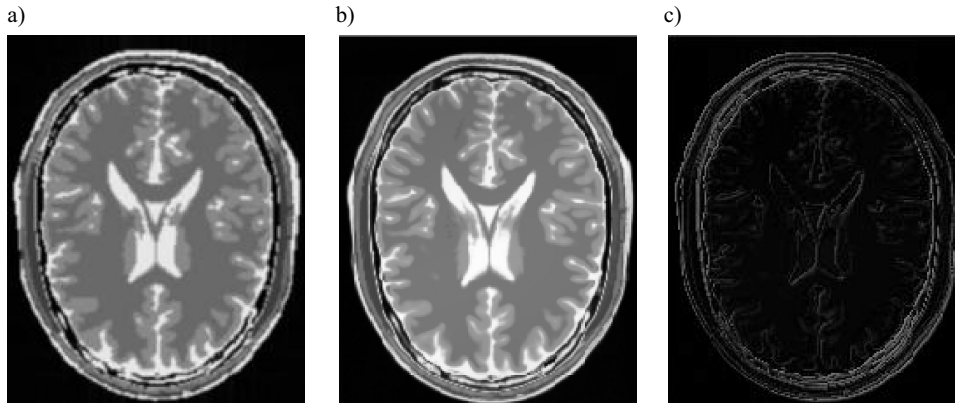
a)   b)   c)

Fig. 8. Validation of the simulator, images generated in a spin echo experiment (TR = 2000ms, TE = 100ms): a) from the presented simulator, b) from the Montreal University simulator and c) difference image (absolute value from difference between image a) and b))

Insignificant differences visible on the difference images are meaningless for tissue contrasting and also tumor detection, even if we simulate the MRI for small structures, as vessels in vascular trees [22].

5.2. Efficiency of the Parallel Implementation

The presented results were obtained in many experiments. Single slice and multislice simulations were performed. The size of the single slice varied between 256×256 and 1024×1024 voxels.

In the experiments a cluster of sixteen SMP servers running Linux 2.6 and connected by an Infiniband network was used. Each server was equipped with two 64-bit Xeon 3.2GHz CPUs with 2MB L2 cache, 2GB of RAM and an Infiniband 10 Gb/s HCA connected to a PCI-Express port. We used the MVAPICH version 0.9.5 [24] as the MPI standard implementation [25].

Figure 9 presents the obtained mean speedup. It is clearly visible that we gain a significant acceleration that is very close to linear. It results both from a short period of time needed for the MPI operations (e.g. sending and receiving messages) and the structure of the proposed model which is characterized by high scalability.

In order to show the significance of the parallel implementation, we present one of the representative results from multislice imaging (see Table 1). It shows the
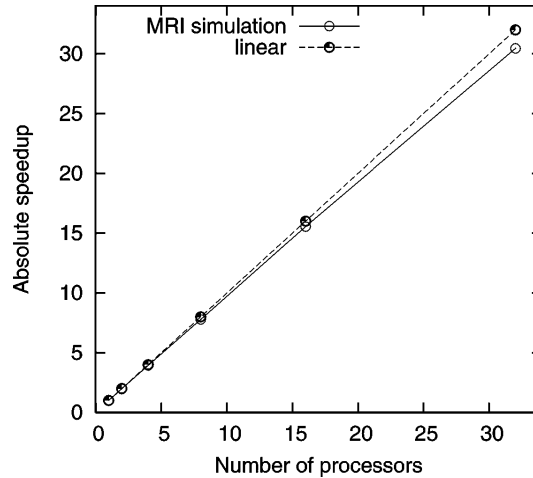
Fig. 9. Efficiency of the parallel implementation: mean speedup for many configurations of the MRI parameters

Table 1.   One of the representative time results (in seconds) from the MRI simulation in the parallel environment, for a different number of processors and various slice thicknesses (size of slice 512×512×slice thickness voxels)

number of processors	1 mm slice	2 mm slice	4 mm slice
1	1470	2895	5749
2	735	1451	2887
4	371	731	1458
8	187	371	735
16	93	183	372
32	48	94	187

dependency of the MRI simulation time on slice thickness (1, 2 or 4 mm) and number of processors. As an example, the time needed to render an image from a slice of 1 mm thickness (512×512 voxels) equals 1470 seconds (about 25 minutes). On the other hand, the simulation in the parallel environment (with 32 processors) can generate the same image approximately 31 times faster (i.e. less than 1 minute). Moreover, it is worth noting that the speedup, in spite of the increasing thickness of the slice, does not decrease significantly. For 32 nodes it still varies around 31. A short time needed to obtain the images in the parallel environment enables the user to operate the presented simulator more easily and more comfortably. Both scientists and students can simulate several images in one minute and consequently several dozens in one hour.

6. Conclusion

In the paper, the virtual scanner of magnetic resonance imaging is presented. Following a review of different approaches to the simulation of magnetic resonance imaging, the simulator aimed at accelerating and simplifying the procedure of virtual image generation is briefly described. We tried to achieve these objectives focusing on the most important NMR principles having the significant influence on tissue contrasting. We parallelized the most complex calculations in the magnetization kernel (signal acquisition process). Moreover, the graphical user-friendly interface was created.

It was experimentally shown that the presented simulator makes possible to generate images which are comparable with results from other more sophisticated (i.e. characterized by higher complexity) virtual scanners. Moreover, the parallel implementation also accelerates the MRI simulation. We gain a significant speedup which is very close to linear. These findings create new perspectives for obtaining more precise images in a reasonable period of time.

The proposed simulator is still under development, as we can see many possible directions for future improvements. Currently, in order to gain wider access to the MRI simulator, an online graphical user interface is being created. Moreover, due to some recently developed MRI methods, a modeling of new MRI sequences seems to be necessary. The implementation of the MRI experiment (relaxations and signal acquisition) within the framework of multi-platform shared-memory parallel programming (OpenMP) can make possible to introduce magnetic dependencies between different slices of the phantom during the multislice imaging process keeping, at the same time, the previously gained speedup. Furthermore, we intend to perform an in-depth validation with real scanners and real phantoms.

References

1. Webb A.G.: Introduction to medical imaging, Wiley-IEEE Press, 2002.
2. Bloch F., Hansen W.W., Packard M.: Nuclear induction. Physical Review 1946, 69, 127.
3. Purcell E.M., Torrey H.C., Pound R.V.: Resonance absorption by nuclear magnetic moments in a solid. Phys. Rev. 1946, 69, 37.
4. Bittoun J., Taquin J., Sauzade M.: A computer algorithm for the simulation of any nuclear magnetic resonance (NMR) imaging method. Magn. Reson. Imaging 1984, 2, 113–120.
5. Summers R.M., Axel L., Israel S.: A computer simulation of nuclear magnetic resonance imaging. Magn. Reson. Med. 1986, 3, 363–376.
6. Olsson M.B.E., Wirestam R., Persson B.R.R.: A computer simulation program for MR imaging: Application to RF and static magnetic field imperfections. Magn. Reson. Med. 1995, 34, 612–617.

7. Brenner A.R., Kursch J., Noll T.G.: Parallelized high-performance MRI simulation on a workstation cluster, Proc. Int. Soc. Magn. Reson. Med. 1997, 3, 2052.
8. Ortendahl D.A., Hylton N., Kaufman L., Watts J.C., Crooks L.E., Mills C.M., Stark D.D.: Analytical tools for magnetic resonance imaging. Radiology 1984, 153, 479–488.
9. Bobman S.A., Riederer S.J., Lee J.N., Suddarth S.A., Wang H.Z., MacFall J.R.: Synthesized MRI images: comparison with acquired images. Radiology 1985, 155, 731–738.
10. Petersson J.S., Christoffersson J.-O., Golman K.: MRI simulation using the k-space formalism. Mag. Reson. Imag. 1993, 11, 557–568.
11. Kwan R.K.S., Evans A.C., Pike G.B.: MRI simulation-based evaluation of image-processing and classification methods. IEEE Trans. Med. Imag. 1999, 18, 1085–1097.
12. Benoit-Cattin H., Collewet G., Belaroussi B., Saint-Jalmes H., Odet C.: The SIMRI project: a versatile and interactive MRI simulator. J. Magn. Reson. 2005, 173, 97–115.
13. Krętowski M., Rolland Y., Bezy-Wendling J., Coatrieux J.-L.: Physiologically based modeling for medical image analysis: application to 3D vascular network and CT scan angiography. IEEE Trans. Medical Imaging 2003, 22, 2, 248–257.
14. Krętowski M., Bezy-Wendling J., Coupe P.: Simulation of biphasic CT findings in hepatic cellular carcinoma by a two-level physiological model. IEEE Trans. Biomed. Eng. 2007, 54, 3, 538–542.
15. Lambert J.B., Mazzola E.P.: Nuclear magnetic resonance spectroscopy: an introduction to principles, applications, and experimental methods, Pearson Prentice Hall, New Jersey 2003.
16. Krętowski M., Bezy-Wendling J.: Modeling for medical image analysis: framework and applications, In: C.T. Leondes (Ed.), Medical Imaging Systems Technology, World Scientific Publishing, 2005, 1–32.
17. Kuperman V.: Magnetic resonance imaging – physical principles and applications, Academic Press, San Diego 2000.
18. Bloch F.: Nuclear induction. Physical Review 1946, 70, 460–474.
19. Twieg D.: The k-trajectory formulation of the NMR imaging process with applications in analysis and synthesis of imaging methods. Med. Phys. 1983, 10, 5, 610–621.
20. Press W.H., Teukolsky S.A., Vetterling W.T., Flannery B.P.: Numerical recipes in C. The art of scientific computing, Cambridge University Press, 1992.
21. Gropp W., Lusk E., Skjellum A.: Using MPI: Portable parallel programming with the message-passing interface, MIT Press, 1999.
22. Bezy-Wendling J., Krętowski M., Mescam M., Jurczuk K., Eliat P.-A.: Simulation of hepatocellular carcinoma in MRI by combined macrovascular and pharmacokinetic models, Proc. of 4th IEEE International Symposium on Biomedical Imaging: From Nano to Macro, Washington USA 2007, 1272–1275.
23. Mescam M., Bezy-Wendling J., Krętowski M., Jurczuk K., Eliat P.-A., Olivie D.: Coupling texture analysis and physiological modeling for liver dynamic MRI interpretation, Proc. 24th IEEE EMBS, Lyon, France 2007, 4223–4226.
24. Liu J., Wu J., Panda D.K.: High performance RDMA-based MPI implementation over InfiniBand. Int. Journal Parallel Program. 2004, 32, 3, 167–198.
25. Juhasz Z., Kacsuk P., Kranzlmuller D.: Distributed and Parallel Systems: Cluster and Grid Computing, Springer, 2005.